AIAA SciTech Forum
8-12 January 2024, Orlando, FL
AIAA SCITECH 2024 Forum

10.2514/6.2024-0653

Spectral Model for Nonequilibrium Radiation Induced from Flow Around a Hypersonic Body

Joseph A. Farmer∗, Andrew A. Oliva †, Ryan G. McClarren ‡, Aleksandar Jemcov§, Joseph M. Powers ¶
Department of Aerospace and Mechanical Engineering
University of Notre Dame, Notre Dame, Indiana, 46556-5637

This study presents a two-dimensional simulation of hypersonic flow around a cylindrical geometry along with the development and verification of a line-by-line emission and absorption spectral database for nonequilibrium flows characterized by two temperatures. The spectral databases have currently been constructed for atomic and molecular species in five-species air-chemical models with translational and vibrational temperatures spanning 300 – 4800 K, number density regimes from 1×10^{10} – 1×10^{20} cm^{-3}, and for spectral ranges in the vacuum ultraviolet and infrared. In order to gather the radiative properties of relevant hypersonic thermodynamic states, we employ a bicubic polynomial interpolation between temperatures and spline interpolation between number densities. The spectral database is accessed with a finite volume Photon Monte Carlo method and the model is verified through reconstruction of absorbtion coefficients and comparisons with exact solutions for radiative transfer in one-dimensional gas mixtures. Then sample radiation calculations are performed on a snapshot in time of the two-dimensional flow where there is substantial energy in both the post-shock zone and wake region.

I. Nomenclature

I	=	radiative intensity (W m^{-2})
κ	=	absorption coefficient (m^{-1})
κ_{tr}	=	translational-rotational thermal conductivity (W m^{-1} K^{-1})
κ_{ve}	=	vibrational-electronic thermal conductivity (W m^{-1} K^{-1})
ϵ	=	emission coefficient (m^{-1})
λ	=	wavelength (m) or dilation viscosity (Pa s)
$\hat{s}$	=	line of sight
$q_{\text{rad},i}$	=	radiative heat flux vector (W m^{-3})
$q_{tr,i}$	=	translational-rotational heat flux vector (W m^{-3})
$q_{ve,i}$	=	vibrational-electronic heat flux vector (W m^{-3})
Ω	=	solid angle
n	=	number of particles
u	=	upper non-degenerate state
l	=	lower non-degenerate state
g	=	degeneracy
B_{lu}	=	Einstein coefficient for stimulated emission (J^{-1} m^3 s^{-2})
B_{ul}	=	Einstein coefficient for absorption (J^{-1} m^3 s^{-2})
A_{ul}	=	Einstein coefficient for spontaneous emission (s^{-1})
h	=	Planck's constant (J s)
c	=	speed of light (m s^{-1})
$\mathcal{R}_\lambda$	=	random number relation for wavelength
$\mathcal{R}$	=	universal gas constant (J mol^{-1} K^{-1})

∗Graduate Student,
†Postdoctoral Scholar,
‡Professor,
§Associate Research Professor,
¶Professor, AIAA Associate Fellow.

s = distance traveled (m)
ρ = density (kg m^{-3})
ρ_s = density of specie s (kg m^{-3})
u_i = velocity vector (m s^{-1})
u = x-direction velocity (m s^{-1})
v = y-direction velocity (m s^{-1})
w = z-direction velocity (m s^{-1})
e = mass specific internal energy (m^2 s^{-2})
e_{tr} = mass specific translational-rotational internal energy (m^2 s^{-2})
E = internal energy (J m^{-3})
E_{ve} = vibrational-electronic internal energy (J m^{-3})
E_t = translational internal energy (J m^{-3})
P = pressure (N m^{-2})
P_e = pressure due to free electrons (N m^{-2})
P_s = partial pressure due to specie s (N m^{-2})
μ = dynamic viscosity (Pa s)
δ_{ij} = Kronecker delta (-)
T = temperature (K)
T_{tr} = translational-rotational temperature (K)
T_{ve} = vibrational-electronic temperature (K)
$T_{ve,s}$ = vibrational-electronic temperature of specie s (K)
k_B = Boltzmann constant (J mol^{-1} K^{-1})
$\Delta_{s,r}$ = binary collision integral (m s)

II. Introduction

Complex aerodynamic and thermal environments in hypersonic flows emerge from various physical processes that occur at different time and length scales. As a vehicle travels at hypersonic speeds, it is met with resistance from the surrounding air which leads to the formation of a shock wave. This shock wave causes the flow to decelerate and compress where collisional-radiative (CR) processes arise and kinetic energy is converted into thermal energy [1–3]. The high temperature gas in the post-shock zone prompts emission and absorption of radiative energy through photon transfer which can modify the chemical and energy makeup of the environment [4–10]. Such conditions are typically highly nongray, and the photon energy transfer depends on the spectral distribution of absorption and emission coefficients of the various participating species in the gas mixture.

Exact solutions for such problems are typically only available in one-dimensional domains. This has prompted the development of a suite of approximate solvers to realize radiative transfer in complex environments. In recent years, it has become possible to perform efficient Monte Carlo-based line-by-line (LBL) accurate radiative transfer calculations in multidimensional reacting flows where the all of the internal energy modes can be characterized by a single temperature [11–14]. In these calculations, the absorption coefficients and so-called wavenumber-random number relations are stored for different species at various thermodynamic states. These relations allow representative photon bundles, or rays, to carry statistically significant wavenumbers which can be found efficiently with a simple uniform random number generator. Originally developed by Wang and Modest [15], a variation of the wavenumber selection scheme has also been applied for hypersonic flows in nonequilibrium [16–19]. Sohn et al. constructed a such a spectral module for emission random number databases based on line-strength factors for emission and absorption coefficients where the electronic state populations for both atoms and molecules were computed on the fly with the quasi-steady state (QSS) assumption. This module was implemented for atomic N and O, and diatomic N_2^+, N_2, O_2, and NO and full flow field calculations were realized with a Monte Carlo method.

This current work presents new simulations of hypersonic flow around a blunt body and develops a spectral database method for nonequilibrium flows characterized by two temperatures and couples it with a Monte Carlo radiation solver. We build a database of absorption and emission coefficients where a multitemperature Boltzmann model is implemented for the electronic state populations. The paper is organized as follows. Section III introduces the computational fluid mechanical model. Section IV introduces the nonequilibrium radiation model, and Section V presents applications of the Monte Carlo radiation solver.

III. Computational fluid mechanical model

A. Governing equations

The unsteady, compressible, non-equilibrium Navier-Stokes equations were discretized and solved with appropriate boundary conditions and geometry, described later. The governing equations were identical to those described in Casseau et al. [20, 21] and are summarized in this section. The various balance equations are shown below in a generalized vector form as

$$\frac{\partial \boldsymbol{\mathcal{U}}}{\partial t} + \frac{\partial}{\partial x_i}\left(\boldsymbol{\mathcal{F}}_{i,\text{inv}} - \boldsymbol{\mathcal{F}}_{i,\text{vis}}\right) = \dot{\boldsymbol{\mathcal{W}}}\,, \tag{1}$$

which assumes a mixture of N_s species and N_m molecules. Here, the first equation is mass conservation, followed by the species balance equations, then x-, y-, and z-direction momentum balances, then the vibrational energy balance, and lastly, a total energy balance. The vector $\boldsymbol{\mathcal{U}}$ contains the conserved quantities and is defined as

$$\boldsymbol{\mathcal{U}} \equiv \begin{pmatrix} \rho \\ \rho_s \\ \rho u \\ \rho v \\ \rho w \\ E_{ve,m} \\ E \end{pmatrix}, \tag{2}$$

where ρ is density, ρ_s is the density of species s, u is the x-direction velocity, v is the y-direction velocity, w is the z-direction velocity, $E_{ve,m}$ is the vibrational-electronic internal energy energy of molecular specie m, and E is the mixture total internal energy. Additional information on the components of the total internal energy E is given later. The vector $\boldsymbol{\mathcal{F}}_{i,\text{inv}}$ contains the inviscid flux terms and is defined as

$$\boldsymbol{\mathcal{F}}_{i,\text{inv}} \equiv \begin{pmatrix} \rho u_i \\ \rho_s u_i \\ \rho u_i u + \delta_{i1} P \\ \rho u_i v + \delta_{i2} P \\ \rho u_i w + \delta_{i3} P \\ E_{ve,m} u_i \\ (E+P) u_i \end{pmatrix}, \tag{3}$$

where u_i is the ith component of the velocity vector, P is the pressure, and δ_{ij} is the Kronecker delta. The vector $\boldsymbol{\mathcal{F}}_{i,\text{vis}}$ contains the diffusive flux terms and is defined as

$$\boldsymbol{\mathcal{F}}_{i,\text{vis}} \equiv \begin{pmatrix} 0 \\ -\mathcal{J}_{s,i} \\ \tau_{i1} \\ \tau_{i2} \\ \tau_{i3} \\ -q_{ve,i,m} - e_{ve,m}\mathcal{J}_{m,i} \\ \tau_{ij}u_j - q_{tr,i} - q_{ve,i} - \sum_{r\neq e} h_r \mathcal{J}_r \end{pmatrix}, \tag{4}$$

where $\mathcal{J}_{s,i}$ is the ith component of the diffusive flux vector for species s, τ_{ij} is the viscous shear stress tensor, $q_{ve,i,m}$ is the ith component vibrational-electronic heat flux vector for molecular speciesi m, $e_{ve,m}$ is the vibrational-electronic mass specific internal energy for molecular species m, $q_{tr,i}$ is the ith component of the translational-rotational heat flux vector, $q_{ve,i}$ is the ith component of the vibrational-electronic heat flux vector, h_r is the enthalpy of formation for species r, and $\mathcal{J}_r$ is the diffusive heat flux for species r.

Each specie is assumed to follow the ideal gas law and Dalton's law of partial pressures as

$$P = \sum_{s \neq e} P_s + P_e = \sum_{s \neq e} \rho_s R_s T_{tr} + \rho_e R_e T_{ve,\text{ref}} \,, \tag{5}$$

where P_s is the partial pressure due to specie s, P_e is due to free electrons, R_s is the specific gas constant for specie s, T_{tr} is the translational-rotational temperature, ρ_e is the mass specific density of free electrons, R_e is the specific gas constant for free electrons, $T_{ve,\text{ref}}$ is the reference vibrational-electronic temperature. A caloric equation of state is discussed in this section after details of the multiple-temperature model used in this work are given.

A Newtonian fluid assumption satisfying Stokes' assumption is used, so the viscous shear stress is

$$\tau_{ij} = \mu \left(\frac{\partial u_i}{\partial x_j} + \frac{\partial u_j}{\partial x_i} \right) - \frac{2}{3} \mu \frac{\partial u_k}{\partial x_k} \delta_{ij} \,, \tag{6}$$

where μ is the dynamic viscosity.

The translational-rotational heat flux vector is defined as

$$q_{tr,i} \equiv \sum_s q_{tr,i,s} = - \sum_s \kappa_{tr,s} \frac{\partial T_{tr}}{\partial x_i} \; \forall s \in N_s \setminus \{e\} \,, \tag{7}$$

where $\kappa_{tr,s}$ is the translational-rotational thermal conductivity of species s. The vibrational-electronic heat flux vector is defined as

$$q_{ve,i} \equiv \sum_s q_{ve,i,s} = - \sum_s \kappa_{ve,s} \frac{\partial T_{ve,s}}{\partial x_i} \; \forall s \in N_s \,, \tag{8}$$

where $\kappa_{ve,s}$ is the vibrational-electronic thermal conductivity of species s. The diffusive flux vector is defined as

$$\mathcal{J}_{s,i} = \begin{cases} \mathcal{I}_{s,i} - Y_s \sum_{r \neq e} I_{r,i} \; \forall (s,r) \in N_s \setminus \{e\}, \\ \mathcal{M}_e \sum_{r \neq e} \frac{C_r \times \mathcal{J}_{r,i}}{\mathcal{M}_r} \text{ otherwise,} \end{cases} \tag{9}$$

where $I_{s,i}$ is defined as

$$\mathcal{I}_{s,i} \equiv -\rho \mathcal{D}_s \frac{\partial Y_s}{\partial x_i} \,. \tag{10}$$

Here, Y_s is the mass fraction of specie s and $\mathcal{D}_s$ is the diffusion coefficient defined as

$$\mathcal{D}_s \equiv (1 - X_s) \left(\sum_{r \neq s} \frac{X_r}{\mathcal{D}_{s,r}} \right)^{-1} \; \forall (s,r) \in N_s \setminus \{e\} \,, \tag{11}$$

where X_s is the molar fraction of specie s. Additionally, C_r is the charge of specie r, and $\mathcal{M}_s$ is the molecular mass of specie s. The symbol $\mathcal{D}_{s,r}$ is the binary diffusion coefficient for species s and r. The binary diffusion coefficient is calculated as

$$\mathcal{D}_{s,r} = \frac{k_B T_{tr}}{P \Delta_{s,r}} \,, \tag{12}$$

where k_B is the Boltzmann constant and $\Delta_{s,r}$ is the binary collision integral.

The source vector $\dot{\boldsymbol{\mathcal{W}}}$ is defined as

$$\dot{\boldsymbol{\mathcal{W}}} \equiv \begin{pmatrix} 0 \\ \dot{\omega}_s \\ 0 \\ 0 \\ 0 \\ \dot{\omega}_{v,m} \\ 0 \end{pmatrix} , \tag{13}$$

where $\dot{\omega}_s$ is the specie s source term due to chemical reactions and $\dot{\omega}_{v,m}$ is the vibrational-electronic energy change due to chemical reactions involving molecular specie m. The $\dot{\omega}_s$ is written as

$$\dot{\omega}_s = \mathcal{M}_s \sum_{r=1}^{N_s} (\nu''_{s,r} - \nu'_{s,r}) \left[k_{f,r} \prod_{k=1}^{N_r} \left(\frac{\rho_k}{\mathcal{M}_k} \right)^{\nu'_{k,r}} - k_{b,r} \prod_{k=1}^{N_r} \left(\frac{\rho_k}{\mathcal{M}_k} \right)^{\nu''_{k,r}} \right] , \tag{14}$$

where $\nu'_{s,r}$ and $\nu''_{s,r}$ are the forward and backward stoichiometric coefficients. The forward reaction rate coefficient k_f is defined as

$$k_f \equiv A T_{c,f}^{\beta} \exp\left(\frac{-T_a}{T_{c,f}} \right) , \tag{15}$$

where A is a pre-exponential factor, β is the controlling-temperature exponent, $T_{c,f}$ is the forward-controlling temperature for the reaction, and T_a is the activation temperature. The backward reaction rates are calculated using the equilibrium constant K_{eq} as

$$k_b = \frac{k_f}{K_{eq}} , \tag{16}$$

where k_b is the backward reaction rate. For additional information on the reaction rates and controlling temperatures, see Park [22, 23].

The vibrational energy exchange term $\dot{\omega}_{v,m}$ is defined as

$$\dot{\omega}_{v,m} \equiv \begin{cases} Q_{m,V-T} + Q_{m,V-V} + Q_{m,C-V} + Q_{m,e-V}, \text{ if the reference molecule for } e \text{ is not } m, \\ Q_{m,V-T} + Q_{m,V-V} + Q_{m,C-V} + Q_{m,e-V} + Q_{h-e} + Q_{e-i} + u_i \frac{\partial P_e}{\partial x_i}, \text{ otherwise,} \end{cases} \tag{17}$$

where $Q_{m,V-T}$ is the trans-rotational and vibro-electronic, $Q_{m,V-V}$ is the vibrational-vibrational, $Q_{m,C-V}$ is the chemical-vibrational, $Q_{m,e-V}$ is the free electron and vibrational, $Q_{m,h-e}$ is the heavy-particle and free electron, and $Q_{m,e-i}$ vibrational and electron impact ionization energy exchange rates. The term $u_i(\partial P_e/\partial x_i)$ is an approximation of the work done to the electrons by the electric field set up by the electron pressure gradient [21]. The trans-rotational and vibro-electronic energy exchange rate is given by the Landau-Teller equation

$$Q_{m,V-T} \equiv \rho_m \frac{e_{ve,m}(T_{tr}) - e_{ve,m}(T_{ve,m})}{\tau_{m,V-T}} \; \forall m \in N_m , \tag{18}$$

where $\tau_{m,V-T}$ is the molar-averaged V-T relaxation time and $e_{ve,m}$ is the vibro-electornic internal energy. This relaxation time contains a contribution from Millikan-White [24] and a Park correction term [22]. The $Q_{m,V-V}$ captures the exchange of vibro-electronic energy during collisions and is defined as

$$Q_{m,V-V} \equiv \sum_{\substack{l \neq m \\ l \neq e}} N_A \sigma_{m,l} \mathcal{P}_{m,l} \sqrt{\frac{8}{\pi} \frac{\mathcal{R}}{\mathcal{M}_{m,l}} T_{tr}} \frac{\rho_l}{\mathcal{M}_l} \rho_m \left(e_{v,m}(T_{tr}) \frac{e_{v,l}(T_{ve,l})}{e_{v,l}(T_{tr})} - e_{v.m}(T_{ve,m}) \right) \; m, l \in N_m , \tag{19}$$

additional details can be found in Casseau et al. [20], Knab et al. [25, 26]. The $Q_{m,C-V}$ captures the vibro-electronic energy exchange rate occurring during chemical reactions and is defined as

$$Q_{m,C-V} \equiv \dot{\omega}_m \left(D'_m + e_{el,m} \right) \; m \in N_m , \tag{20}$$

where

$$D'_m = \begin{cases} e_{ve,m}, \text{ if non-preferential model is used} \\ \alpha_m D_m, \text{ if preferential model is used,} \end{cases} \tag{21}$$

for additional details see [27–29]. The remaining terms $Q_{m,e-V}$, $Q_{m,h-e}$, $Q_{m,e-i}$ are all assumed to be zero as in Casseau et al. [20, 21].

The total internal energy E is defined as

$$E \equiv \frac{1}{2} \rho \sum_i u_i^2 + \sum_{s \neq e} E_{t,s} + \sum_{s \neq e} E_{r,s} + \sum_{s \neq e} E_{v,s} + \sum_{s \neq e} E_{el,s} + E_e + \sum_{s \neq e} \rho_s h_s^o , \tag{22}$$

where u_i is the velocity vector, $E_{t,s}$ is the translational energy of specie s, $E_{r,s}$ is the rotational energy of species s, $E_{v,s}$ is the vibrational energy of species s, $E_{e,s}$ is the electronic energy of species s, E_e is the free electron internal energy, and h_s^o is the enthalpy of formation for specie s. This work follows Casseau et al. [20, 21] and uses the Park TTv model [23] such that the translational and rotational energies are assumed to be in equilibrium and, therefore, utilize a single temperature, i.e.,

$$E_{tr} = \sum_s \rho_s e_{tr,s} = \sum_s \rho_s (e_{t,s}(T_{tr}) + e_{r,s}(T_{tr})) = \sum_s \rho_s \frac{5}{2} R_s T_{tr} \ . \tag{23}$$

Further, note that the single translational-rotational temperature T_{tr} is the same for the mixture regardless of the specie s. Similarly, the vibrational and electronic internal energies are also assumed to be in equilibrium so that they also share a single temperature, i.e.,

$$E_{ve} = \sum_s \rho_s e_{ve,s} = \sum_s \rho_s (e_{v,s}(T_{ve,s}) + e_{el,s}(T_{ve,s})) \ , \tag{24}$$

where $e_{v,s}$ is the vibrational internal energy of specie s and $e_{el,s}$ is the electronic internal energy of specie s.

The caloric equation of state relating the specific heat at constant pressure c_P to the enthalpy h is given by Gupta et al. [30]. Further, the caloric equation of state is used to determine the temperatures T_{tr} and $T_{ve,s}$ given information about the enthalpy h_s as calculated by the vibrational energy and total energy balances. The form of the enthalpy for specie s is given as

$$h_s(T) = \left(A_{1,s} T + \frac{A_{2,s}}{2} T^2 + \frac{A_{3,s}}{3} T^3 + \frac{A_{4,s}}{4} T^4 + \frac{A_{5,s}}{5} T^5 + A_{6,s} \right) \mathcal{R} \ , \tag{25}$$

where $A_{1,s}$, $A_{2,s}$, $A_{3,s}$, $A_{4,s}$, $A_{5,s}5$, and $A_{6,s}$ are empirically determine coefficients specific to each specie s and $\mathcal{R}$ is the universal gas constant. The species vibrational enthalpy $h_{ve,s}$ can be calculated as

$$h_{ve,s}(T_{ve,s}) = h_s(T_{ve,s}) - (c_{P,\text{trans},s} + c_{P,\text{rot},s})(T_{ve,s} - T_{\text{ref}}) - h_s^o, \tag{26}$$

where h_s is the enthalpy for specie s (i.e., translational, rotational, vibrational, and electronic), $c_{P,\text{trans},s}$ is the specific heat at constant pressure due to translation, $c_{P,\text{rot},s}$ is the specific heat at constant pressure due to rotation, and h_s^o is the enthalpy of formation for specie s [30]. The translational and rotational specific heats at constant pressure are calculated as

$$c_{P,\text{trans},s} = \frac{5}{2} \mathcal{R} \ , \tag{27}$$

and

$$c_{P,\text{rot},s} = \begin{cases} \frac{3}{2}\mathcal{R} \text{ for a non-linear molecules,} \\ \mathcal{R} \text{ for a linear molecules, and} \\ 0 \text{ for monatomic species.} \end{cases} \tag{28}$$

Thus, the enthalpy for specie s (i.e., the sum of translational, rotational, vibrational, and electronic) for the two-temperature model may then be calculated as

$$h_s(T_{tr}, T_{ve,s}) = h_{ve,s}(T_{ve,s}) + (c_{P,\text{trans},s} + c_{P,\text{rot},s})(T_{tr} - T_{\text{ref}}) + h_s^o \ . \tag{29}$$

The respective internal energy values could be calculated by subtracting the contribution of $\rho_s R_s T_{tr}$ from the respective enthalpy components. Thus, this allows the vibrational non-equilibrium flows to be used with the existing empirical fits for enthalpy for various species.

B. Discretization

The equations given above in this section govern the physics of hypersonic flow. The discretization of these equations is given in Greenshields et al. [31] and is summarized next. The flux terms of the governing equations are discretized as

$$\int_{\mathcal{V}} \frac{\partial}{\partial x_i}(u_i \Psi)\, d\mathcal{V} = \int_S \Psi u_i n_i\, dS \approx \sum_f S_f u_f n_f \Psi_f = \sum_f S_f \phi_f \Psi_f, \tag{30}$$

where $\mathcal{V}$ is the cell volume and Ψ is the quantity being advected with the fluid, n_i is the area unit normal direction, and S_f is the surface area of face f, and ϕ_f is the volumetric flux $\phi_f = u_f n_f$. The fluid property Ψ is linearly interpolated from the owner cell and a neighboring cell based on the characteristics of compressible flow

$$\sum_f \phi_f \Psi_f = \sum_f \left(\alpha \phi_{f+} \Psi_{f+} + (1-\alpha)\phi_{f-} \Psi_{f-} + \omega_f \left(\Psi_{f-} - \Psi_{f+} \right) \right) , \tag{31}$$

where transported quantities following the '+' and the '−' characteristics are indicated with a subscript and go into and out of the cell face, α is a weighting to be described later, and ω_f is the diffusive volumetric flux. The term Ψ_f is defined as

$$\Psi_{f+} = \max \left[c_{f+}|S_f| + \phi_f, c_{f-}|S_f| + \phi_{f-} \right] , \tag{32}$$

where $c_{f\pm}$ is the speed of sound. The weighting factor α is defined as

$$\alpha \equiv \begin{cases} 1/2, \text{ if the Kurganov-Tadmor method,} \\ \frac{\Psi_{f+}}{\Psi_{f+}+\Psi_{f-}}, \text{ for the Kurganov-Noelle-Petrova method.} \end{cases} \tag{33}$$

The diffusive volumetric flux is calculated as

$$\omega_f \equiv \begin{cases} \alpha \max \left[\Psi_+, \Psi_- \right], \text{ for the Kurganov-Tadmor method,} \\ \alpha(\alpha - 1) \left(\Psi_{f+} + \Psi_{f-} \right), \text{ for the Kurganov-Noelle-Petrova method.} \end{cases} \tag{34}$$

Limiters are implemented using r for the f_+ direction as

$$r \equiv 2 \frac{d_i \cdot (\frac{\partial}{\partial x_i} \Psi_i)_{\text{Owner}}}{\Psi_{\text{Neighbor}} - \Psi_{\text{Owner}}} - 1, \tag{35}$$

where d_i is the distance vector between the owner and neighbor cell centers. The interpolation of the positive and negative characteristics is based on limiting the first-order upwind and second-order linear interpolation. The limiters were chosen as total variation diminishing and symmetric [31].

$$\Psi_{f+} = (1 - g_{f+}) \Psi_{\text{Owner}} + g_{f+} \Psi_{\text{Neighbor}} , \tag{36}$$

where $g_{f+} = \beta(1 - \omega_f)$. Different values of β produce different interpolations. For example, $\beta = 0$ gives upwind interpolation while $\beta = 1$ gives linear interpolation, and $\beta = 2$ gives downwind interpolation for $\beta = \frac{r+|r|}{1+r}$ or $\beta = \max(0, \min(1, r))$. A discussion on the gradient and Laplacian term discretizations and other details is given in Greenshields et al. [31].

IV. Nonequilibrium radiation model

Radiative energy transfer exhibits spatial, angular, and frequency dependence and is considered quasi-steady for the problems under consideration because the time scales which govern hydrodynamic and chemical phenomena are comparatively much longer. Therefore propagation of radiative energy can be described by the radiative transfer equation (RTE) which is expressed as

$$\hat{s} \cdot \nabla I_\lambda = \epsilon_\lambda - \kappa_\lambda I_\lambda, \tag{37}$$

in a nonscattering medium. This form of the RTE is an ordinary differential equation for radiative intensity I_λ along a line of sight $\hat{s}$ and is valid for a given wavelength λ. The right hand side describes how intensity is augmented by emission (ϵ_λ) and attenuated by absorption ($\kappa_\lambda I_\lambda$). Energy conservation within participating media can be represented by the divergence of the radiative heat flux

$$\frac{\partial q_{\text{rad},i}}{\partial x_i} = \int_0^\infty \left(4\pi\epsilon_\lambda - \int_{4\pi} \kappa_\lambda I_\lambda \, d\Omega \right) d\lambda, \tag{38}$$

which describes the net energy loss from a control volume by integrating the intensity and emission and absorption coefficients over all wavelengths and solid angles Ω. Therefore a comprehensive treatment of radiative transfer requires the resolution of the spatial, angular, and frequency dependence and the determination of emission and absorption coefficients.

Radiative transfer can be resolved via the finite volume Photon Monte Carlo (PMC) method. The PMC method mimics radiative transfer via the emission and tracing of statistically meaningful photon bundles. These photon bundles are initialized with an emission origin, direction, and wavelength through so-called random number relations. Photon bundles are uniformly distributed within each finite volume cell and are released isotropically. Emission wavelengths are selected by comparing a uniformly distributed random number, $\mathcal{R}_\lambda$, to the probability density function

$$\mathcal{R}_\lambda = \frac{\int_0^{\lambda_\gamma} \epsilon_\lambda \, d\lambda}{\int_0^{\infty} \epsilon_\lambda \, d\lambda}. \tag{39}$$

where a bisection method resolves the equality. This procedure ensures that wavelengths at strong emitting locations are most likely to be chosen. Moreover, each photon bundle carries a finite amount of energy proportional to the total volumetric emission,

$$E_{\text{tot}} = \int_V \int_0^{\infty} \int_{4\pi} \epsilon_\lambda \, d\Omega \, d\lambda \, dV, \tag{40}$$

and the total number of photon bundles emitted from the cell volume V. Once a photon is assigned an emission location, direction, wavelength, and initial energy content, it is ejected from its origin and traced through the domain where it deposits an amount of energy ΔE into the local medium as it traverses a distance s by

$$\Delta E = E^0 \left(1 - e^{-\kappa_\lambda s}\right), \tag{41}$$

where E^0 is the photon bundles initial energy content. Each photon bundle is active until it leaves the computational domain or its energy is depleted.

The absorption and emission and emission coefficients can be determined by

$$\kappa_\lambda = \left(g_l n_l B_{lu} - g_u n_u B_{ul}\right) \frac{h}{\lambda} \phi_\lambda, \tag{42}$$

$$\epsilon_\lambda = g_u n_u A_{ul} \frac{hc}{\lambda 4\pi}, \tag{43}$$

where a number of particles, n, are at nondegenerate upper (u) and lower (l) energy states with g degeneracy, and A_{ul} is the Einstein coefficient for spontaneous emission, B_{ul} is the Einstein coefficient for stimulated emission, B_{lu} is the Einstein coefficient for absorption, hc/λ represents the photon energy given Planck's constant h and speed of light c, and ϕ_λ is a line shape function which describes how the spectral line is broadened. Equation (42) is the effective volumetric absorption coefficient obtained in terms of the stimulated emission and absorption while Eq. (43) represents the spontaneous emission coefficient [32]. To resolve Eq. (38), it is necessary to determine the strength of all spectral lines. In local thermodynamic equilibrium, these can be computed a priori because the electronic state populations are described by Boltzmann's distribution. In nonequilibrium, one has to employ an appropriate method to compute the number of particles at the upper and lower energy states. To that end, we select the NonEQuilibrium AIr Radiation (NEQAIR) software package developed by Whiting et al. [22, 33, 34]. We set the NEQAIR code to a multitemperature Boltzmann model and produce the emission and absorption spectrum at the various thermodynamic states described by Table 1.

Under the proposed framework, we generate emission and absorption databases for use in nonequilibrium flows characterized by two temperatures. Since emission from each individual species is not affected by the emission of other species, the total emission can be represented as summation of each species individual contribution, [35]. Therefore, we develop databases for the species generated from five-species air-chemical models, i.e., NO, N_2, O_2, N, O. Each database is constructed according to Eq. (39) so that a single database contains the wavelength-random number relation and the emission and absorption coefficients for 16 distinct translational and vibrational temperatures and 11 different densities. In order to reconstruct the absorption coefficient at a thermodynamic state in between the database points, bicubic (third-degree) polynomial interpolation for the two temperatures, and spline interpolation between densities.

Parameters	Range and values
Species	N, O, NO, N_2, O_2
Spectral range	85.5 – 200, 0.0005 nm;
	1500 – 7500, 0.005 nm
n	1×10^{10} – 1×10^{20} cm^{-3},
	for every order of magnitude
T_t	300 – 4800, 300 K
T_v	300 – 4800, 300 K

Table 1 Thermodynamic states of LBL database

V. Results and discussion

A. Verification of nonequilibrium thermal radiation model

The nonequilibirum radiation spectral model was first evaluated by reconstruction of the absorption coefficients with the PMC method for NO and atomic N. A thermodynamic state is set for both cases where $n = 2.00666 \times 10^{16}$ cm^{-3}, $T_t = 4100$ K, and $T_v = 3800$ K. The Monte Carlo code was set to sample 1×10^5 rays. In order to reproduce the absorption coefficient, a spline is constructed between the absorption coefficient at neighboring density databases, where a sample at each of the nearest temperature databases is used to perform bicubic interpolation at the current gas temperature. Figure 1 shows good agreement between samples and the curve produced by NEQAIR at the given thermodynamic state. A small spectral interval in the infrared is shown for NO in Fig. 1a while Fig. 1b shows a small window in the vacuum ultraviolet for atomic N.

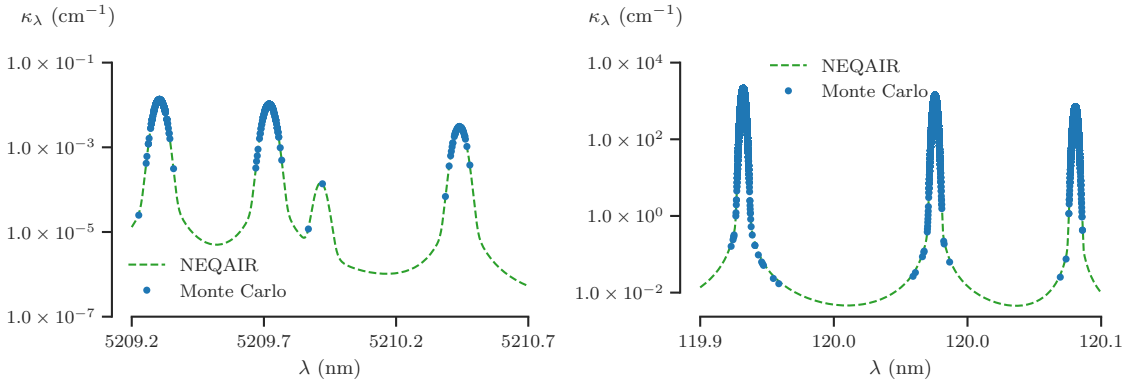

(a) Absorption coefficient of NO **(b) Absorption coefficient of atomic N**

Fig. 1 Comparison of absorption coefficient between Monte Carlo spectral module and NEQAIR results

Next the model is applied to a one-dimensional gas slab bounded by two parallel black walls. Modest [7] gives the exact solution for the heat flux for this configuration in equilibrium. In nonequilibrium, the source term which contains the Planck's function $I_{b\lambda}$, or blackbody intensity, is replaced by the nonequilibrium source of $\epsilon_\lambda/\kappa_\lambda$. Two test cases are constructed compare the divergence of heat flux between the exact method and the Monte Carlo method. Absorption and emission coefficients are again produced by NEQAIR. Both test cases consider a domain size 0.1 cm with discretized by 24 finite volumes, and $n = 2.00666 \times 10^{16}$ cm^{-3}, $T_t = 4100$ K, $T_v = 3800$ K set as the local thermodynamic state in each cell. Figure 2 compares the two solutions where Fig. 2a considers only NO participating in the infrared spectral range, and Fig. 2b considers only N participating in the vacuum ultraviolet spectral range. The Monte Carlo method was run with 1×10^5 rays for five statistical runs and the error bars represent one standard deviation from the mean. Good agreement is shown where the exact solution is always within the error bars for both cases.

The final verification result for the new spectral database is a one-dimensional gas mixture of of N_2, NO, O, O_2, and N. The temperatures and scaler fields are chosen to be similar to the Crew Exploration Vehicle (CEV) line of sight

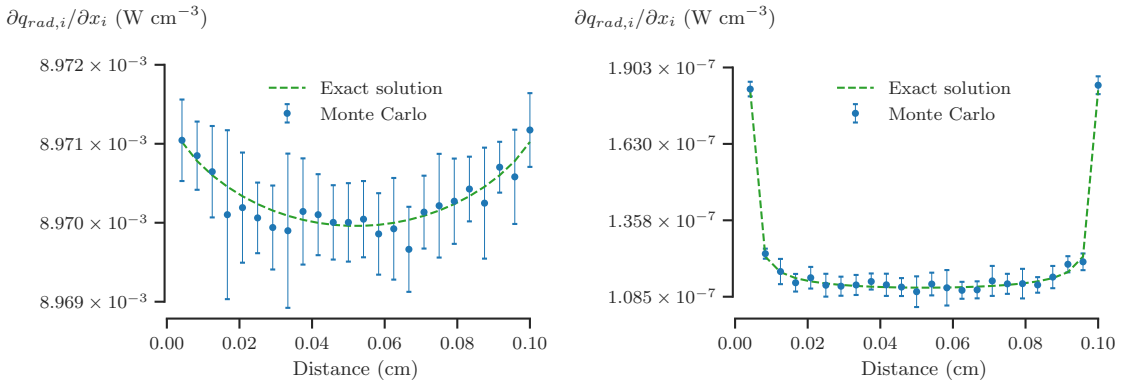

(a) Solution with NO in infrared spectral range **(b) Solution with N in vacuum ultraviolet spectral range**

Fig. 2 Comparison of $\frac{\partial q_{\mathbf{rad},i}}{\partial x_i}$ for hot gas mixture with Monte Carlo method and the analytical solution

data from NEQAIR. The CEV case offers a large range of temperatures Fig. 3a and densities Fig. 3b, and a region of strong nonequilibrium near the shock for which to test the spectral database. For this case the divergence of heat flux is compared with NEQAIR's implementation of the exact solution given by Modest. The Monte Carlo code was again run with 1×10^5 rays for five statistical runs and only emission from the vacuum ultraviolet is considered. The result in Fig. 3 shows good agreement with the exact solution. In this case, a small region near the body has greater absorption than emission.

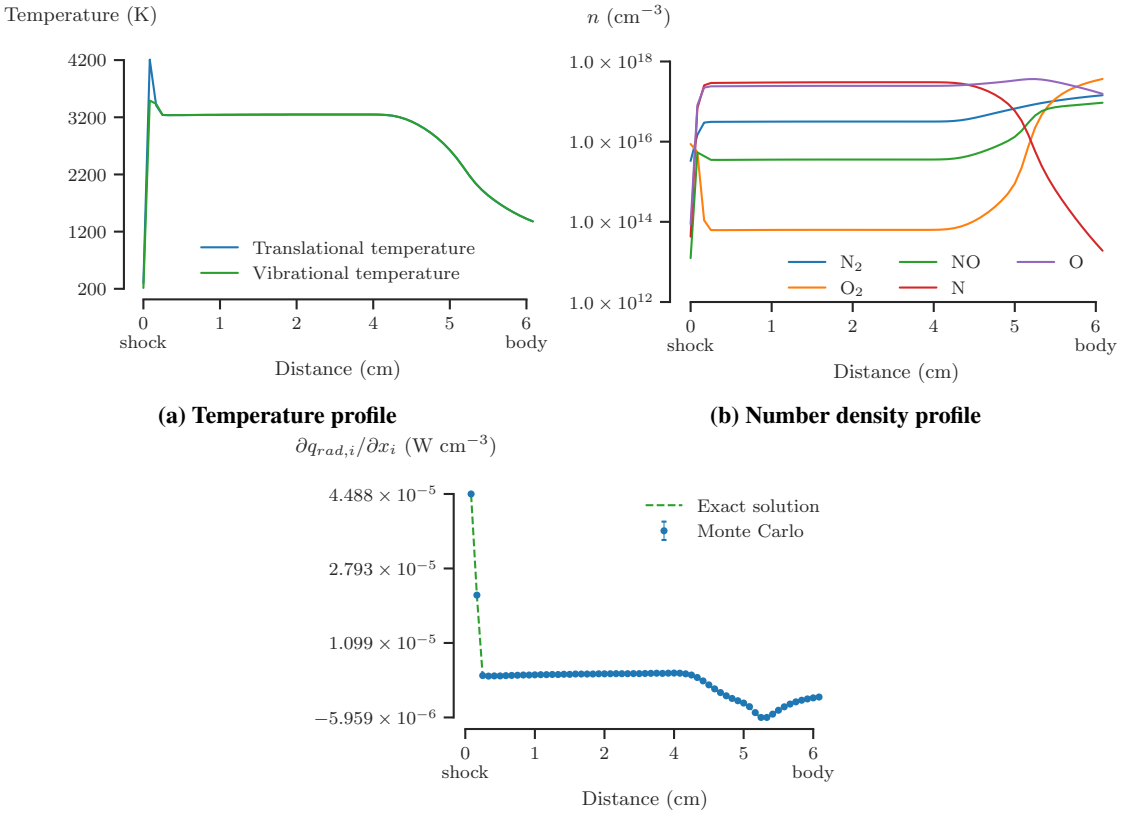

(a) Temperature profile **(b) Number density profile**

(c) Solution considering vacuum ultraviolet spectral range

Fig. 3 Radiative transfer solution of a representative thermodynamic state of hypersonic flow

B. Hypersonic flow with dissociation

We simulate the hypersonic flow of air over a cylinder. The model equations are the compressible reactive Navier-Stokes equations. We model air as an ideal mixture of multiple monatomic and diatomic species, and we do not allow for ionization. A two-temperature model is employed that captures the translational and vibrational kinetic energy of the component gases. A multicomponent diffusion model is employed for species diffusion, and we use standard mixture models for momentum and energy diffusion. The model is solved in a computational environment based on the OpenFOAM computational simulation tool running in a massively parallel environment. The schematic of the domain geometry and computational mesh are shown in Fig. 4. The boundary conditions for the free stream were set based on an altitude of 24.384 (km), that is, $U_\infty \approx 2682$ m/s, $P_\infty \approx 2802$ Pa, and $T_\infty \approx 221$ K. The computational mesh contains a thin layer of hexahedral cells surrounding the two-dimensional cylinder to accurately capture the boundary layer dynamics. Beyond this layer, the mesh is comprised of polyhedral cells. The total mesh contained 17,050 hexahedral cells and 21,489 polyhedral cells, amounting to 38,539 cells in total. Sample predictions of translational and vibrational temperatures are shown in Fig. 3a. Mass fraction profiles for NO, O, and N, are shown in Fig. 5c, 5d, 5e, respectively, and the mixture density is shown in Fig. 5f. The radiative emission and absorption are illustrated in Fig. 6. It can be observed the radiative emission closely follows the high vibrational tempearture regions, as well as the mass fractions for NO, N, and O. The absorption coefficient has similar structures, but similar to the final verification case, the regions which are not as energy dense have more absorption than emission.

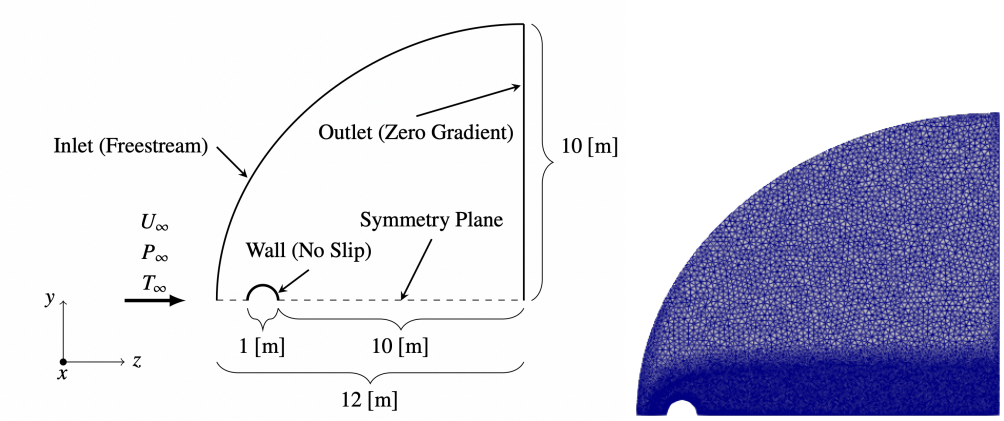

(a) Schematic of computational domain and geometry **(b) Mesh of simulation domain**

Fig. 4 Mesh and schematic of simulation domain

VI. Conclusion

In this study, we introduced a simulation of hypersonic flow over a bluff body, coupled with the development of a spectral module integrated with a photon Monte Carlo method. Because of nonequilibrium flow conditions, we formulated a dual-temperature database that spans relevant species, and ranges in density and frequency space. To verify the solver, the absorption coefficients were reproduced for a given thermodynamic state and the divergence of radiative heat flux was compared for a variety of one dimensional problems where the exact solution could be computed. This model is easily extended to the more complex simulations and is applied to the 2D flow over a cylinder. In this case, there was high energy in the post-shock zone and in the wake region. This represents a large spatial volume which the Monte Carlo code needs to compute. The primary benefit of the strategy is that radiative emission is received practically for free as it is received directly from the pretabulated spectral database. However, in order to compute the the mixture absorption coefficient, the ray tracing is charged with 16 more look-ups per cell per ray. In order to reduce the look-ups per cell, we can consider exploring a default to a pure equilibrium strategy if the vibrational and translational temperatures are close in magnitude.

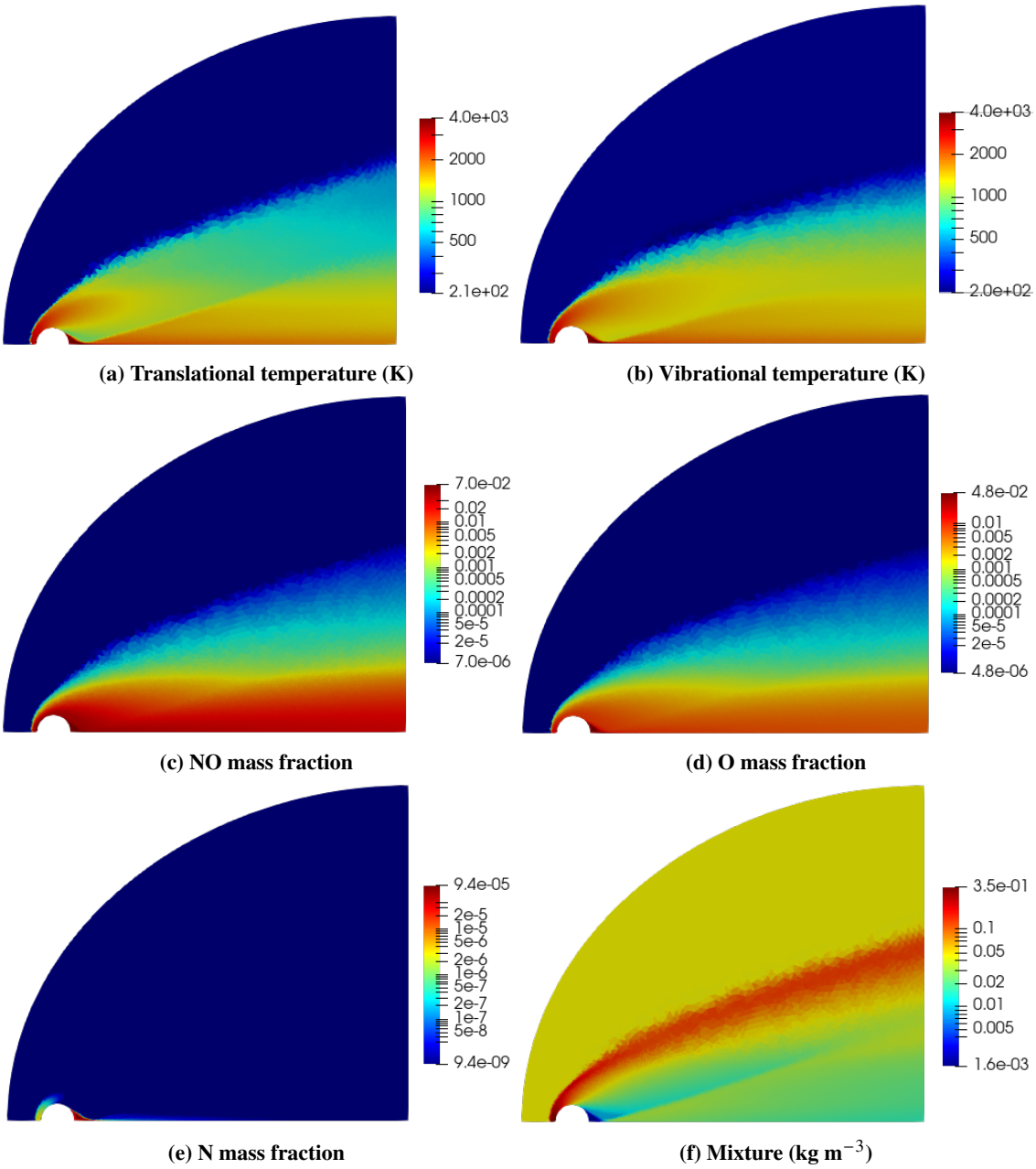

(a) Translational temperature (K) **(b) Vibrational temperature (K)**

(c) NO mass fraction **(d) O mass fraction**

(e) N mass fraction **(f) Mixture (kg m^{-3})**

Fig. 5 Thermodynamic state of flow field

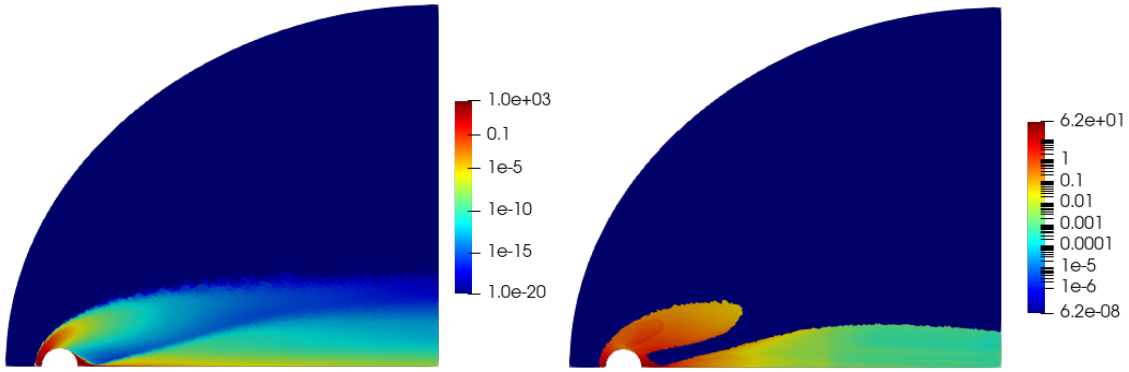

(a) Radiative emission (W m^{-3}) **(b) Radiative absorption (W m^{-3})**

Fig. 6 Comparison of radiative emission and absorption for a 2D flow with significant energy in the shock and wake region

References

[1] Zel'dovich, Y., and Raizer, Y., *Physics of Shock Waves and High-Temperature Hydrodynamic Phenomena*, Dover, Mineola, New York, 2012.

[2] Gnoffo, P. A., "Planetary-Entry Gas Dynamics," *Annual Review of Fluid Mechanics*, Vol. 31, No. 1, 1999, pp. 459–494. https://doi.org/10.1146/annurev.fluid.31.1.459.

[3] Sahai, A., Johnston, C. O., Lopez, B., and Panesi, M., "Comparative Analysis of Reduced-Order Spectral Models and Grouping Strategies for Non-Equilibrium Radiation," *Journal of Quantitative Spectroscopy and Radiative Transfer*, Vol. 242, 2020, p. 106752. https://doi.org/https://doi.org/10.1016/j.jqsrt.2019.106752, URL https://www.sciencedirect.com/science/article/pii/S0022407319306983.

[4] Anderson, J. D., "An Engineering Survey of Radiating Shock Layers." *AIAA Journal*, Vol. 7, No. 9, 1969, pp. 1665–1675. https://doi.org/10.2514/3.5373.

[5] Goulard, R., "The Coupling of Radiation and Convection in Detached Shock Layers," *Journal of Quantitative Spectroscopy and Radiative Transfer*, Vol. 1, No. 3, 1961, pp. 249–257. https://doi.org/https://doi.org/10.1016/0022-4073(61)90025-5.

[6] Li, G., and Modest, M. F., "Importance of Turbulence-Radiation Interaction in Turbulent Diffusion Flames," *Journal of Heat Transfer*, Vol. 125, 2003, pp. 831 – 838. https://doi.org/10.1115/1.1597621.

[7] Modest, M. F., *Radiative Heat Transfer*, Academic Press, San Diego, 2013.

[8] Johnston, C. O., Brandis, A. M., and Panesi, M., "Refinements to Afterbody Radiative Heating Simulations for Earth Entry," AIAA 2016-3693, 46th AIAA Thermophysics Conference, 2016. https://doi.org/10.2514/6.2016-3693.

[9] Brandis, A. M., Johnston, C. O., and Cruden, B. A., "Nonequilibrium Radiation for Earth Entry," AIAA 2016-3690, 46th AIAA Thermophysics Conference, 2016. https://doi.org/10.2514/6.2016-3690.

[10] Johnston, C. O., and Panesi, M., "Impact of State-Specific Flowfield Modeling on Atomic Nitrogen Radiation," *Physical Review Fluids*, Vol. 3, 2018, p. 013402. https://doi.org/10.1103/PhysRevFluids.3.013402.

[11] Ren, T., and Modest, M. F., "Line-by-Line Random-Number Database for Monte Carlo Simulations of Radiation in Combustion System," *Journal of Heat Transfer*, Vol. 141, No. 2, 2018. https://doi.org/10.1115/1.4041803, 022701.

[12] Farmer, J., and Roy, S., "A Quasi-Monte Carlo Solver for Thermal Radiation in Participating Media," *Journal of Quantitative Spectroscopy and Radiative Transfer*, Vol. 242, 2020, p. 106753. https://doi.org/https://doi.org/10.1016/j.jqsrt.2019.106753.

[13] Wu, B., Roy, S. P., and Zhao, X., "Detailed Modeling of a Small-Scale Turbulent Pool Fire," *Combustion and Flame*, Vol. 214, 2020, pp. 224–237. https://doi.org/https://doi.org/10.1016/j.combustflame.2019.12.034.

[14] Roy, S., Cai, J., and Modest, M., "Development of a Multiphase Photon Monte Carlo Method For Spray Combustion and its Application In High-Pressure Conditions," *International Journal of Heat and Mass Transfer*, Vol. 115, 2017, pp. 453–466. https://doi.org/10.1016/j.ijheatmasstransfer.2017.07.046.

[15] Wang, A., and Modest, M., "Spectral Monte Carlo models for nongray radiation analyses in inhomogeneous participating media," *International Journal of Heat and Mass Transfer*, Vol. 50, 2007, pp. 3877–3889. https://doi.org/10.1016/j.ijheatmasstransfer.2007.02.018.

[16] Sohn, I., "Modeling and Simulation of Radiation from Hypersonic Flows using Monte Carlo Methods," Ph.D. thesis, Pennsylvania State University, Feb. 2011.

[17] Ozawa, T., Modest, M. F., and Levin, D. A., "Spectral Module for Photon Monte Carlo Calculations in Hypersonic Nonequilibrium Radiation," *Journal of Heat Transfer*, Vol. 132, No. 2, 2009. https://doi.org/10.1115/1.4000242, 023406.

[18] Ozawa, T., Levin, D. A., Wang, A., and Modest, M., "Development of Coupled Particle Hypersonic Flowfield- Photon Monte Carlo Radiation Methods," *Journal of Thermophysics and Heat Transfer*, Vol. 24, No. 3, 2010, pp. 612–622. https://doi.org/10.2514/1.44645.

[19] Feldick, A., and Modest, M. F., "An Improved Wavelength Selection Scheme for Monte Carlo Solvers Applied to Hypersonic Plasmas," *Journal of Quantitative Spectroscopy and Radiative Transfer*, Vol. 112, No. 8, 2011, pp. 1394–1401. https://doi.org/ https://doi.org/10.1016/j.jqsrt.2011.01.028, URL https://www.sciencedirect.com/science/article/pii/S0022407311000537.

[20] Casseau, V., Palharini, R. C., Scanlon, T. J., and Brown, R. E., "A Two-Temperature Open-Source CFD Model for Hypersonic Reacting Flows, Part One: Zero-Dimensional Analysis," *Aerospace*, Vol. 3, No. 4, 2016. https://doi.org/10.3390/aerospace3040034.

[21] Casseau, V., Espinoza, D. E. R., Scanlon, T. J., and Brown, R. E., "A Two-Temperature Open-Source CFD Model for Hypersonic Reacting Flows, Part Two: Multi-Dimensional Analysis," *Aerospace*, Vol. 3, No. 4, 2016. https://doi.org/10.3390/aerospace3040045.

[22] Park, C., *Nonequilibrium Hypersonic Aerothermodynamics*, John Wiley and Sons Inc, New York, 1990.

[23] Park, C., "Review of Chemical-Kinetic Problems of Future NASA Missions. I - Earth Entries," *Journal of Thermophysics and Heat Transfer*, Vol. 7, No. 3, 1993, pp. 385–398. https://doi.org/10.2514/3.431.

[24] Millikan, R. C., and White, D. R., "Systematics of Vibrational Relaxation," *The Journal of Chemical Physics*, Vol. 39, No. 12, 1963, pp. 3209–3213. https://doi.org/10.1063/1.1734182.

[25] Knab, O., Fruehauf, H.-H., and Jonas, S., "Multiple Temperature Descriptions of Reaction Rate Constants with Regard to Consistent Chemical-Vibrational Coupling," AIAA-1992-2947, 27th AIAA Thermophysics Conference, 1992. https://doi.org/10.2514/6.1992-2947.

[26] Knab, O., Fruehauf, H.-H., and Messerschmid, E. W., "Theory and Validation of the Physically Consistent Coupled Vibration-Chemistry-Vibration Model," *Journal of Thermophysics and Heat Transfer*, Vol. 9, No. 2, 1995, pp. 219–226. https://doi.org/10.2514/3.649.

[27] Marrone, P. V., and Treanor, C. E., "Chemical Relaxation with Preferential Dissociation from Excited Vibrational Levels," *Physics of Fluids*, Vol. 6, No. 9, 1963, pp. 1215–1221. https://doi.org/10.1063/1.1706888.

[28] Gnoffo, P. A., Gupta, R. N., and Shinn, J. L., "Conservation Equations and Physical Models for Hypersonic Air Flows in Thermal and Chemical Nonequilibrium," Tech. Rep. 19890006744, NASA, 1989.

[29] Scalabrin, L. C., "Numerical Simulation of Weakly Ionized Hypersonic Flow Over Reentry Capsules," Ph.D. thesis, The University of Michigan, 2007.

[30] Gupta, R. N., Yos, J. M., Thompson, R. A., and Lee, K.-P., "A Review of Reaction Rates and Thermodynamic and Transport Properties for an 11-Species Air Model for Chemical and Thermal Nonequilibrium Calculations to 30000 K," Tech. Rep. 19900017748, NASA, 1990.

[31] Greenshields, C. J., Weller, H. G., Gasparini, L., and Reese, J. M., "Implementation of Semi-Discrete, Non-Staggered Central Schemes in a Colocated, Polyhedral, Finite Volume Framework, for High-Speed Viscous Flows," *International Journal for Numerical Methods in Fluids*, Vol. 63, No. 1, 2010, pp. 1–21. https://doi.org/https://doi.org/10.1002/fld.2069.

[32] Goody, R. M., and Yung, Y. L., *Atmospheric Radiation: Theoretical Basis*, Oxford University Press, New York, 1989.

[33] Whiting, E., Park, C., Liu, Y., Arnold, J., and Paterson, J., *NEQAIR96,Nonequilibrium and Equilibrium Radiative Transport and Spectra Program: User's Manual*, NASA, Reference Publication 1389, 1997.

[34] Cruden, B. A., and Brandis, A. M., "Measurement of Radiative Nonequilibrium for Air Shocks Between 7 and 9 km/s," *Journal of Thermophysics and Heat Transfer*, Vol. 34, No. 1, 2020, pp. 154–180. https://doi.org/10.2514/1.T5735.

[35] Ren, T., and Modest, M. F., "A Hybrid Wavenumber Selection Scheme for Line-By-Line Photon Monte Carlo Simulations in High-Temperature Gases," *Journal of Heat Transfer*, Vol. 135, No. 8, 2013. https://doi.org/10.1115/1.4024385, 084501.